Realizing Saturable Absorption and Reverse-saturable Absorption in PEDOT:PSS Film via Electrical Modulation

Yanhui Sun, [†] Hui Li, [†] Ruipeng Hou, [†] Mengjuan Diao, [†] Ying Liang, [†] Zhipeng Huang, [†*] Mark G. Humphrey, [‡] Chi Zhang [†*]
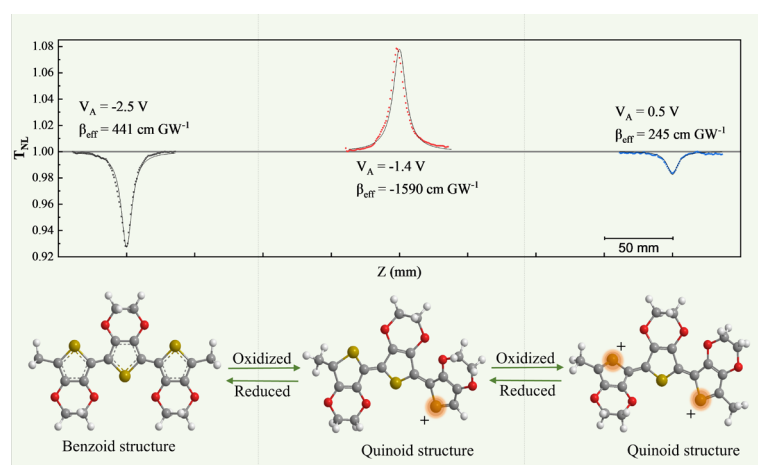
[†] School of Chemical Science and Engineering, Tongji University, Shanghai, 200092, PR China

[‡] Research School of Chemistry, Australian National University, Canberra, ACT 2601, Australia

[*]Corresponding authors: Z.P. Huang (zphuang@tongji.edu.cn),

C. Zhang (chizhang@tongji.edu.cn)

TOC Graphic

Abstract

The electrical tuning of the nonlinear absorption of materials has promising application potential, while studies remain rare. In this work, we show that the third-order nonlinear absorption of poly(3,4-ethylenedioxythiophene) chemically doped with poly(styrene sulfonic acid) [PEDOT:PSS] can be effectively modulated by external voltage. The

nonlinear absorption of the film can be varied between reverse saturable absorption (RSA) and saturable absorption (SA) via voltage control with laser excitation at 800 nm, and corresponding nonlinear absorption coefficient can be tuned in the range -1590 to 518 cm GW^{-1}. The doping level and energy structure of PEDOT are modulated with different voltages. The undoped film affords two-photon absorption and accordingly the RSA response. A moderately doped sample has two polaron levels, and Pauli blocking associated with these two polaron levels results in SA. The bipolaron level in heavily doped PEDOT leads to excited state absorption and therefore RSA behavior. The approach reported here can be applied to other semiconductors, being a convenient, effective, and promising method for the electrical tuning of the optical nonlinearity.

Keyword

PEDOT, conductive polymer, nonlinear optical, electrical control, polaron

1. Introduction

Dynamical modulation of materials' property, especially via electric stimulus, is the fundamental principle of a variety of application, including data storage, signal process, display, communication, etc. The electrical modulating of optical nonlinearity is attracting intensive attention, due to the wide application range of laser.[1,2] Study concerning the electrical modulation of optical nonlinearity can be traced back several decades, but a high electrical field (kilovolts/cm) is necessary to induce noticeable modulation.[3] The electrical field has been remarkably reduced recently because

advanced nano-machining enables fine control over the size and arrangement of active materials. The nonlinear optical (NLO) responses have been electrically modulated in a series of nanostructure, including the plasmonic structures of gold,[4–7] graphene,[8] and silicon,[9] as well as two-dimensional layered structures (WSe_2,[10] $MoTe$,[11] MoS_2,[12] graphene[13]), CdS nanobelt,[14] organic conjugated polymer,[15] etc. However, most efforts have been devoted to modulate the frequency conversion of laser, which is a parametric NLO response.

In a nonparametric NLO process, the transfer of electrons from one real level to another level occurs, and nonlinear absorption is a typical nonparametric NLO process that has extensive application.[16–19] The modulation of nonlinear absorption by external stimuli has been demonstrated. One of us has modulated the nonlinear absorption properties of a series of Ru-based molecular inorganic compounds by electrochemical treatment.[20–23] Hou and Song et al. have tuned the nonlinear absorption of Rhodamine B salicylaldehyde hydrazone metal complex by UV irradiation.[24] However, these studies focused on molecules dispersed in solution. The dynamical tuning of the nonlinear absorption of a solid film is highly desirable for on-chip optoelectrical application, while it has not been reported so far.

In this work, the electrical modulation of the nonlinear absorption of a thin film of poly(3,4-ethylenedioxythiophene) chemically doped with poly(styrene sulfonic acid) [PEDOT:PSS] is studied. PEDOT:PSS is a conductive polymer becoming a subject of intense interest (e.g. organic electrochemical transistors[25], electrochromic devices[26], neural electrodes[27], surface switch devices[28], electronic plants,[29] etc.), because it can be

coupled with ionic and electronic charge species to control the electronic, physical, and chemical properties of material.[30] We show here that the nonlinear absorption of the PEDOT:PSS film can be varied between reverse saturable absorption (RSA) and saturable absorption (SA) via voltage control with laser excitation at 800 nm, and corresponding nonlinear absorption coefficient (β_{eff}) can be tuned in the range -1590 to 518 cm GW^{-1}. An electrochemical process occurs during the variation of applied voltage (V_A), resulting in different doping states of PEDOT:PSS (undoped, moderately doped, and heavily doped). The RSA is ascribed to two-photon absorption (TPA) in the undoped state and excited-state absorption (ESA) in the heavily doped state, and the SA is ascribed to Pauli blocking in the moderately doped PEDOT:PSS. The approach introduced here is convenient and effective, and can be applied to the electrical tuning of the NLO response of other materials.

2. Results and Discussion
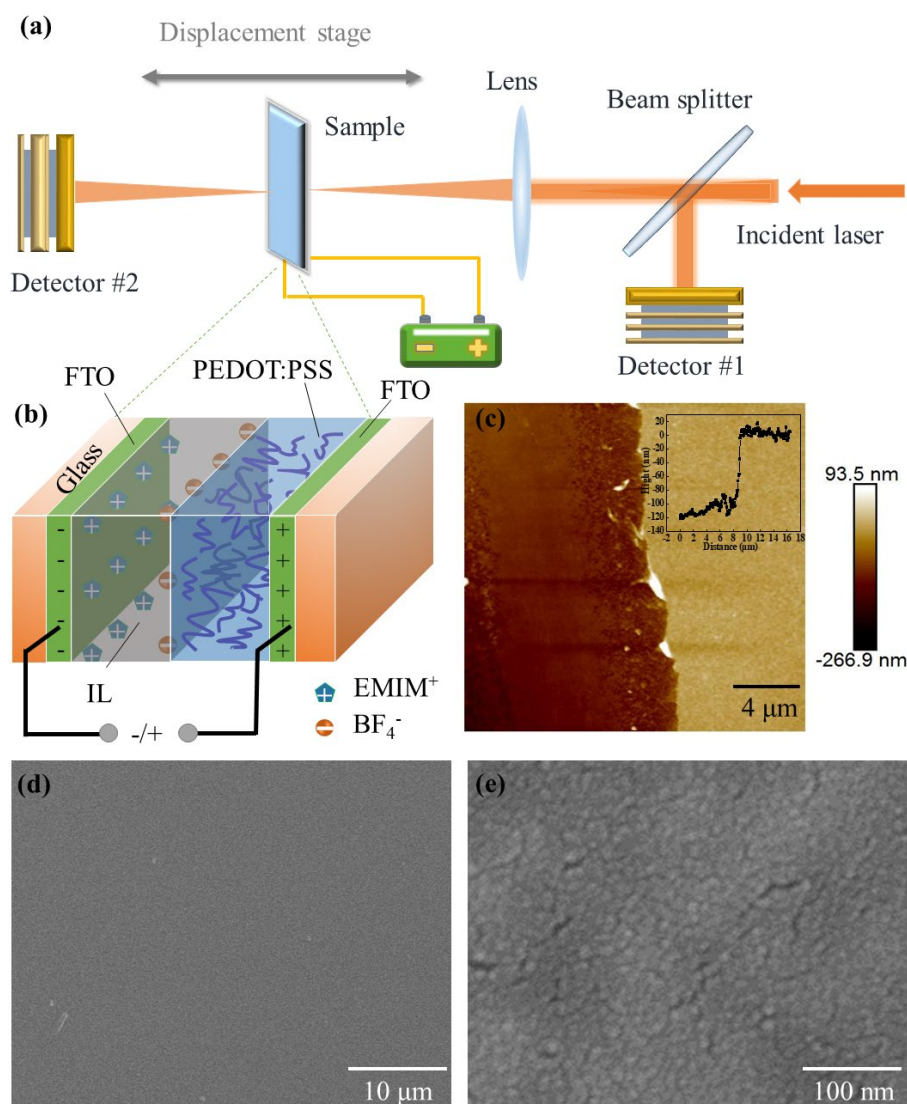
2.1 Device Structure

Figure 1. (a) Schematic of an open-aperture Z-scan setup. (b) Schematic structure of PEDOT:PSS device. (c) AFM image of PEDOT:PSS film and corresponding height profile. (d, e) SEM images of PEDOT:PSS film.

The NLO response of the PEDOT:PSS film is modulated via electrochemical treatment, basing on the fact that electrochemical treatment will vary the electronic structure of the PEDOT:PSS. The experimental setup is illustrated by Figure 1a, composing an open-aperture Z-scan setup and a power supply applying a desirable

voltage to the PEDOT:PSS film. The PEDOT:PSS loaded onto a fluorine-doped tin oxide (FTO) substrate acts as a working electrode, and was assembled into a miniature electrochemical cell, with another FTO substrate serving as a counter electrode, and ionic liquid (IL) as an electrolyte. The IL used is 1-ethyl-3-methylimidazolium tetrafluoroborate (EMIM BF_4). A Surlyn® membrane (60 μm thick) was used to space and bind two electrodes. A typical digital camera image of a device for the Z-scan measurement is shown in Figure S1 in the supporting information (SI). The charging state of the PEDOT:PSS film under positive voltage is schematically illustrated in Figure 1b. When voltage is applied the energy levels and/or bands of PEDOT will be varied due to the reduction or oxidation of PEDOT. Meanwhile, the occupation of these energy levels and/or bands will be also modified. The modification of energy levels/bands and their occupation will initiate different NLO responses, resulting in the electrochemical modulation of the NLO response of the PEDOT:PSS film.

Atomic force microscopy (AFM) was used to characterize the quality and thickness of PEDOT:PSS film. Figure 1c and Figure S2 in SI show that the PEDOT:PSS film is smooth and homogeneous. A cross-sectional height profile near the scratch edge (inset of Figure 1c) indicates that the thickness of the film is *ca* 120 nm. Scanning electron microscopy (SEM) images confirm the homogeneity f PEDOT:PSS films (Figure 1d, and 1e).
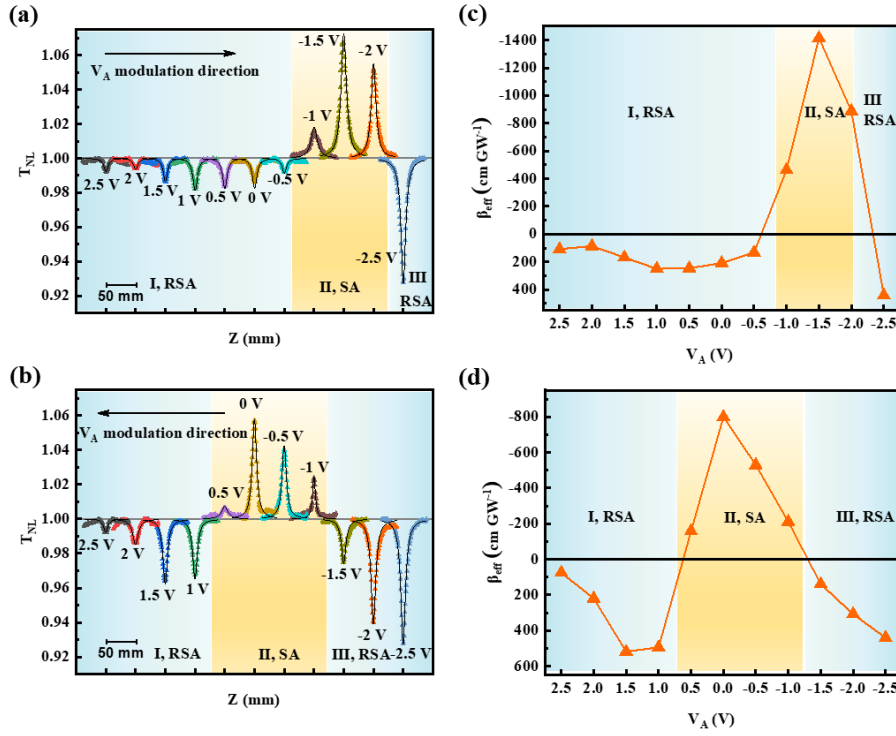
2.2 Electrical Modulation of the NLO Response

Figure 2. Z-scan curves of device at 800 nm under V_A varying (a) from 2.5 V to -2.5 V and (b) from -2.5 V to 2.5 V. The β_{eff} values of the devices under V_A varying (c) from 2.5 to -2.5 V and (d) from -2.5 to 2.5 V.

The electrical modulation of the NLO response of devices was investigated by an open-aperture Z-scan setup. The voltage was applied to the cell for a sufficiently long time to achieve an equilibrium charging state (*i.e.* stable linear transmittance), and then Z-scan was carried out with the same V_A. A series of V_A were applied to the cell, with forward V_A modulation referencing to decrease V_A and backward V_A modulation to increase V_A. The V_A was varied in the range -2.5 V to 2.5 V to avoid possible degradation of the IL. In each Z-scan experiment, the normalized transmittance (T_{NL}) of the device was measured as a function of distance to the focal point of the lens (Z).

The corresponding $T_{NL}(Z)$ curves are plotted in Figure 2a and 2b, which show that the NLO response of the PEDOT:PSS film can be controllably modified via V_A. In both

forward (Figure 2a) and backward V_A modulation (Figure 2b), three V_A regions can be defined according to the NLO response of PEDOT:PSS. For forward V_A modulation The PEDOT:PSS film shows RSA response with V_A in the range 2.5 to -0.5 V (Region I), in which the $T_{NL}(Z)$ decreases with sample closer to the focus of laser (*i.e.* larger laser intensity). The PEDOT:PSS film exhibits SA behavior in V_A region II (-1 to -2 V). In this case, the $T_{NL}(Z)$ increases as the sample closer to the focus. In region III (-2.5 V) the NLO response of PEDOT transforms to RSA. It will be discussed below that different NLO responses are associated with different structures and doping features of PEDOT in the film. In backward V_A modulation, there are also three regions (Figure 2b), while the V_A range is different from those in forward V_A modulation. As shown in the Figure S3 in the SI, the variation of $T_{NL}(Z)$ of a bare device (a device assembled by two bare FTO substrates and injected with IL) with different V_A is negligible in comparison with the PEDOT:PSS device, confirming that the variation of optical nonlinearity comes exclusively from the V_A modulation of PEDOT:PSS.

The effective third-order nonlinear absorption coefficient (β_{eff}) was derived from $T_{NL}(Z)$ curves via data fitting (Experimental section). The results are shown in Figure 2c for forward V_A modulation and Figure 2d for backward V_A modulation. The β_{eff} can be monotonically modulated via V_A between the maximum and the minimum. For forward V_A modulation, the β_{eff} firstly increases from 100 to 300 cm GW^{-1} with decreasing V_A to 1 V, and then β_{eff} monotonically decreases to -1415 cm GW^{-1} with further V_A decreasing to -1.5 V. Beyond this value the β_{eff} increases with decreasing V_A. The backward V_A modulation shows a similar feature. The close correlation between

β_{eff} and V_A enables the on-demand modulation of the NLO performance of the PEDOT. The largest value of β_{eff} from modulated PEDOT:PSS film is -1590 cm GW^{-1} achieved with a V_A of -1.4 V (Figure S4a in the SI). The β_{eff} of typical semiconductor materials showing SA response are listed in Table 1. It is shown that the maximum value of the β_{eff} of PEDOT:PSS is larger than those of most semiconductors with laser excitation at 800 nm wavelength. Meanwhile, the Z-scan experiments were carried out with the V_A repeatedly varied between -1.4 V and 1 V (Figure S4b in the SI), demonstrating that the modulation of β_{eff} is reversible.

Table 1. NLO parameters of typical semiconductors

Materials	λ (nm)	β_{eff} (cm GW^{-1})	Type of NLO
ITO[31]	1240	~ -7500	**SA**
$Cu_{2-x}S$[32]	1300	-161	SA
ITO-5[33]	1500	-51.40	SA
ITO-12[33]	1300	-47.03	SA
Bi_2O_2Se[34]	800	-2910	SA
Bi_2O_2Se[34]	1500	-648	SA
CuS[35]	1030	-1.015 ± 0.007	SA
WS_2[36]	800	-397 ± 40	SA
Black Phosphorus[37]	800	-0.0138	SA
MoS_2[38]	800	$-(4.60 \pm 0.27) \times 10^{-3}$	SA
graphene[39]	800	-20	SA
graphene oxide[39]	800	-40	SA
$AgInSe_2$ nanorods[40]	800	-0.29	SA
Au nanorods[41]	800	-1.5	SA
PEDOT:PSS (this work)	800	-1590	SA

The PEDOT shows hysteresis in β_{eff}-V_A characteristics when the V_A was swept in sequential forward and backward V_A modulation. This is a typical hysteresis effect occurring in electric double layer charged transistor or liquid gate transistor, which arises from the slow electrochemical process PEDOT associated with V_A modulation.[42]
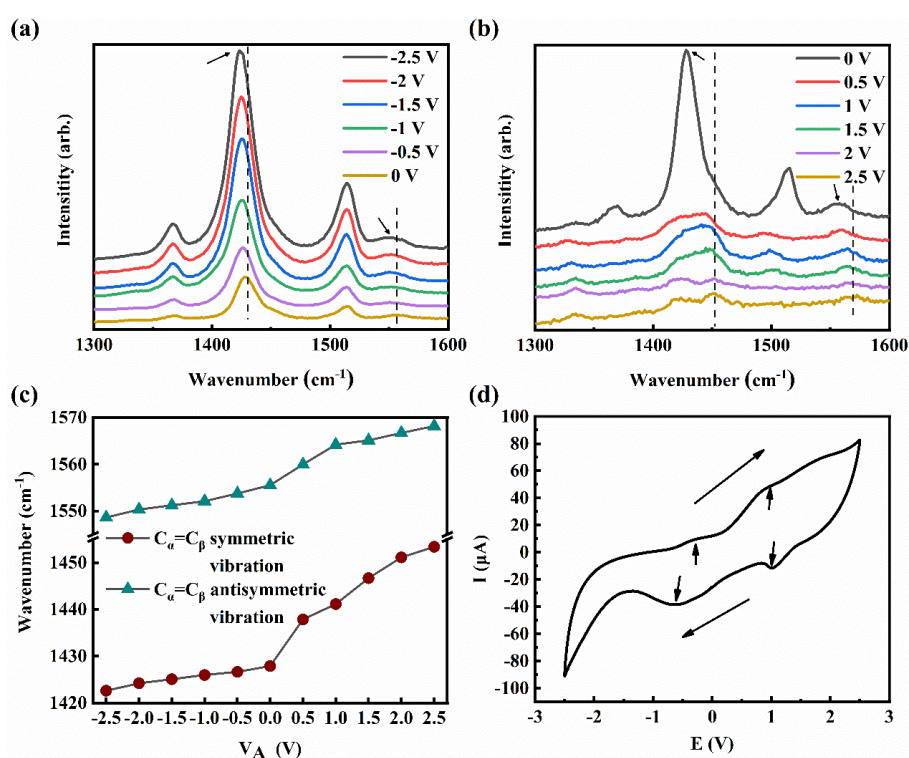
2.3 Process during Electrical Modulation

Figure 3. (a,b) *In-situ* Raman spectra of PEDOT:PSS film for V_A varying in the range -2.5 to 2.5 V. (c) The shift of Raman peaks with V_A. (d) CV of PEDOT:PSS.

The β_{eff}-V_A characteristic of PEDOT:PSS film should be associated with the modulation of the electron state PEDOT, and both electrostatic doping or electrochemical doping might possibly modulate the electron state of PEDOT. In electrostatic doping, an electric double layer forming at the interface of dielectrics and solid functions as a nanoscale capacitor that charges and/or discharges the solid via a non-faradaic process. Differently, the charging and discharging are accomplished by

the oxidation and reduction of material during electrochemical doping. The *in-situ* Raman experiment, cyclic voltammetry (CV), and Vis-NIR spectroscopy suggest that the V_A-related NLO response of the PEDOT:PSS film arises from the electrochemical doping of the PEDOT.

The structural variation of PEDOT under different V_A is indicated by *in-situ* Raman spectra. The *in-situ* Raman spectra are shown in Figure 3a and Figure 3b for backward V_A modulation, and the spectra are plotted in the wavenumber range of 1300 to 1600 cm^{-1} to show clearly the shift of Raman peaks. When a V_A of -2.5 V was applied, $C_\alpha=C_\beta$ antisymmetric vibrations and $C_\alpha=C_\beta$ symmetric vibrations were located at 1548 cm^{-1} and 1422 cm^{-1},[43] respectively. With the V_A gradual increasing, both $C_\alpha=C_\beta$ antisymmetric vibrations and $C_\alpha=C_\beta$ symmetric vibrations were shifted toward larger wavenumber. Finally, the $C_\alpha=C_\beta$ antisymmetric vibrations and $C_\alpha=C_\beta$ symmetric vibrations were shifted to 1568 and 1453 cm^{-1} for a V_A of 2.5 V. Meanwhile, the peaks corresponding to positive V_A are much weaker than those corresponding to negative V_A. This is associated with the electronic screen of photons resulting from the high conductivity of positive charged PEDOT.[44] The detailed variation of the $C_\alpha=C_\beta$ antisymmetric vibrations and $C_\alpha=C_\beta$ symmetric vibrations are plotted in Figure 3c, showing clearly the linear variation of the Raman peaks with the V_A. The *in-situ* Raman spectra in backward V_A modulation (Figure S5 in the SI) is identical to that in forward modulation. The variation of Raman peaks evidences that the structure of PEDOT was modified due to external V_A. These changes are consistent with the transformation of

the benzoid structure into quinoid one upon doping, because in this case the $C_\alpha = C_\beta$

force constant will decrease. [45]

CV experiment confirms the redox process of the PEDOT. Figure 3d shows the

cyclic voltammograms of the PEDOT:PSS film. The cyclic voltammograms of IL on a

bare device (Figure S6a in the SI) show that no apparent redox peak can be found,

indicating that the redox peaks found in Figure 3d are associated with the oxidation and

reduction of the PEDOT. The oxidation peak near a V_A of -0.3 V and the reduction peak

near a V_A of -0.7 V suggest that the redox process occurs during V_A variation. The

oxidation peak near a V_A of 1.1 V and the reduction peak near a V_A of 1 V suggest

another redox process. In the oxidation cycle, the first peak (-0.3 V) corresponds to the

removal of the first electron from the polymer, and thus to the generation of polaron-

dominated mid-gap states.[46] The second peak (1.1 V) corresponds to the removal of the

second electron with the generation of bipolaron-dominated states. In the oxidation

cycle, two peaks also correspond to bipolaron and polaron state, respectively. The

repeated cyclic voltammograms of the PEDOT (Figure S6b in the SI) show that the
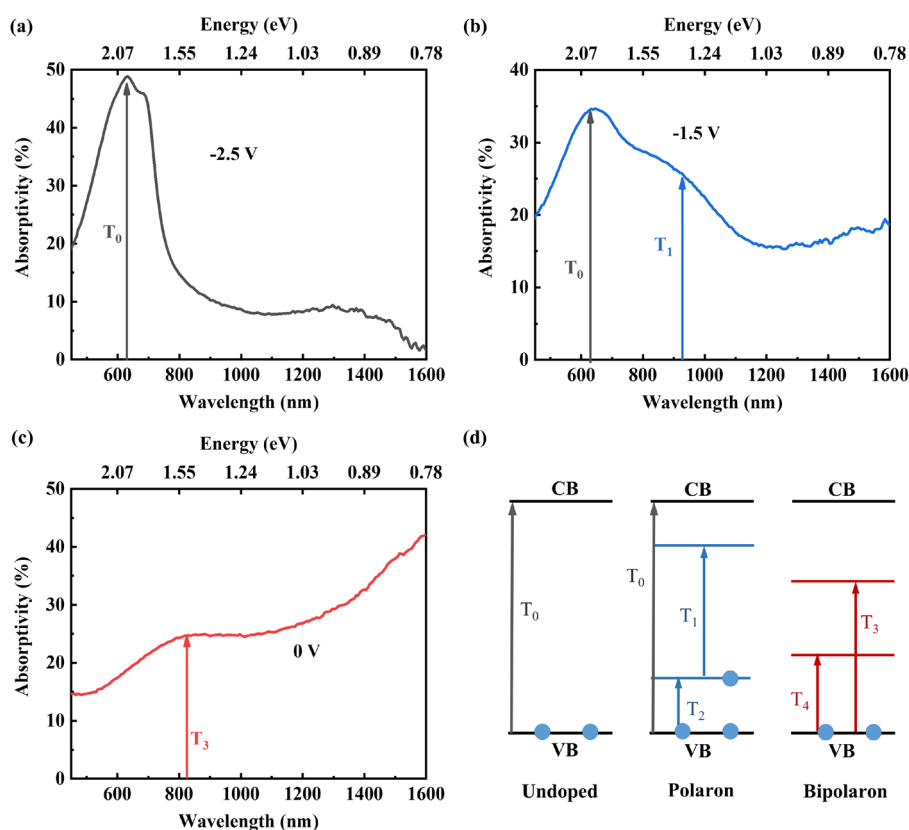
oxidation and reduction of the PEDOT is highly reversible.

Figure 4. Absorption spectra corresponding to different doping levels of PEDOT: (a) undoped (-2.5 V), (b) moderately doped (-1.5 V), and (c) heavily doped (0 V). (d) A proposed schematic of energy level of PEDOT for different doping levels.

The band structure variation during electrochemical doping can be derived from steady-state absorptance spectra corresponding to different doping states. Figure S7a and S7b in the SI show the Vis-NIR absorption spectra of the PEDOT:PSS film with forward and backward V_A modulation, respectively. Similar to those suggested by Raman spectra, the absorption spectra show prominently hysteretic characteristics. Three typical absorption spectra are shown in panel a, b, and c of Figure 4, and a proposed schematic of energy level is drawn as Figure 4d corresponding to each doping state. With a V_A of -2.5 V, the PEDOT:PSS show a peak near ~2 eV (Figure 4a) that can be ascribed to the π- π* electron transition (T_0) of the undoped sample. The corresponding energy is referenced as the bandgap energy (E_g) of PEDOT.[47] With V_A increasing, transition in addition to π- π* electron transition can be found because of

the presence of polaron or bipolaron levels located in the bandgap, and the absorption associated with π-π* electron transition decreases. [47] With a V_A of -1.5 V, the absorption spectrum of PEDOT:PSS shows an apparent shoulders centered at 1.33 eV (Figure 4b). This transition is denoted as T_1, which can be associated with the transition of the first polaron level to the second polaron level because the first polaron level is semi-filled. [48] Meanwhile, the electron initially located at the valance band can also be excited to the first polaron level. This transition is denoted as T_2 (< 0.5 eV), [49,50] while it cannot be detected in our experiment due to the wavelength range of our instrument. With the V_A further increasing, the polaron levels are transformed to the bipolaron states in heavily doped PEDOT. [51] For a heavily doped sample which exhibits two bipolaron states, the only excitation from valence band to the second bipolaron level can be detected (T_3, 1.44eV), and transition between two bipolaron states is absent because the first bipolaron state is nearly empty. [48] The transition of valance band electron to the first bipolaron level is denoted as T_4, which was below 0.5 eV and cannot be detected here.[49,50] It is worth noting that the V_A range of the oxidation/reduction of PEDOT:PSS suggested by UV-Vis experiment to some extend deviates from that shown in Figure 3d. The deviation is associated with the fact that in UV-Vis spectroscopy the voltage was applied to the sample for a sufficiently long time, while in CV experiment the variation of V_A is much faster.

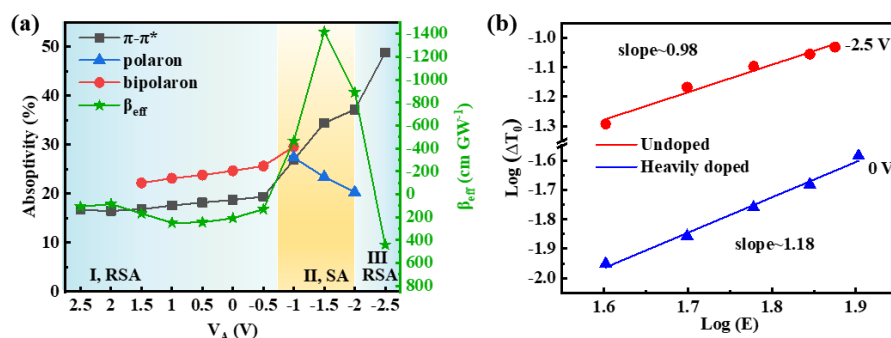## 2.4 Mechanism of the Electrical Tuning of Optical Nonlinearity

Figure 5. (a) The π-π^*, polaron, and the bipolaron absorptivity of the PEDOT:PSS film, as well as the NLO absorption coefficient of PEDOT:PSS film with forward V_A modulation; (b) The relationship of ΔT_0 and laser pulse energy (E) in log-log scale for the PEDOT:PSS film with the V_A of -2.5 V and 0 V, respectively. The data are recorded in the forward V_A modulation.

In order to correlate the NLO response of the PEDOT:PSS film with different voltages to the electronic state of the PEDOT, the linear absorptivity at the wavelengths corresponding to π-π^* transition, polaron-related transition, and bipolaron-related transition are shown together with β_{eff} as a function of V_A in forward V_A modulation (Figure 5a). In region I (V_A in the range 2.5 V to -0.5 V) the PEDOT shows an RSA response, and in this case, the linear absorption comes primarily from T_3 associated with the transition of π electrons to the second bipolaron state/band. With the V_A in the range -1.0 and -2.0 V (region II), strong SA can be detected. In this region the contribution of polaron transition becomes prominent. In region III (a V_A of -2.5 V), the sample shows again RSA response. Only π-π^* transition can be found in the absorption spectra. The relationship between NLO response and the absorptivity at the wavelengths corresponding to π-π^* transition, polaron-related transition, and bipolaron-related transition in backward V_A modulation (Figure S8 in the SI) resembles

well that in forward modulation. The NLO response in region I and III confirms that π-π^* transition and bipolaron-related transition would be responsible for the RSA, while SA can be ascribed to polaron-related transition. The compromise between polaron-related transition and π-π^* transition at the boundary between region II and region III and that between polaron-related transition and bipolaron-related transition at the boundary between region I and region II result in the smallest β_{eff} (strongest SA) in the center of region II.

In the V_A region where the PEDOT shows SA response, the PEDOT exhibits intensive linear absorption at the wavelength of NLO measurement. In general, SA could arise from Pauli blocking with band filling and/or ground state depletion,[52] or the red shift of absorption peak associated with electron temperature raising in the sample because of strong plasmon resonance absorption.[31] Here the Pauli blocking would be the major origin of SA, because the linear absorption at 800 nm in this V_A region has been associated with the transition from the lower polaron level to higher polaron level (T_1 in Figure 4d). For moderately doped PEDOT, the density of polaron states is low, and the lower polaron level is semi-filled. The excitation will heavily deplete the electrons in the lower polaron level, and the band fill effect of the higher polaron state is prominent. These two effects both result in Pauli blocking and therefore SA. SA associated with ground-state depletion of in-gap states is in good accordance with those reported in Fe_2O_3 and WO_3.[53,54]

To confirm that the RSA in regions I and III are the third-order nonlinearity, the Z-scan experiments were carried out with the laser excitation with different pulse energies.

The normalized transmittance changes (ΔT_0, the depth of the valley of $T_{NL}(Z)$ curves) are plotted as a function of laser pulse energy (E) in the log-log scale (Figure 5b). Linear fitting results in a slope of 0.98 for a V_A of -2.5 V and 1.14 for a V_A of 0 V, indicating that the nominal TPA occurs with these V_A and the responses indeed be the third-order optical nonlinearity.[55,56] For the V_A of -2.5 V, π-π* transition is dominant, and the E_g satisfies the relationship $hv < E_g < 2\,hv$, where h is Planck constant and v is the frequency of the laser. Therefore, the RSA in the region III can be associated with a TPA process. The PEDOT:PSS film also shows an RSA response under V_A where the bipolaron-related excitation prevails (Region I). In this case, the energy of the incident photon (hv) is sufficiently large to excite π electrons in valence band (VB) to the second bipolaron level/band (T_3 in Figure 4d), the absorption cross-section of second bipolaron level/band is larger than that of valence band so that the electron excited from VB to bipolaron level or band can be further excited to the conduction band (CB). Namely, ESA is responsible for RSA for heavily doped PEDOT.
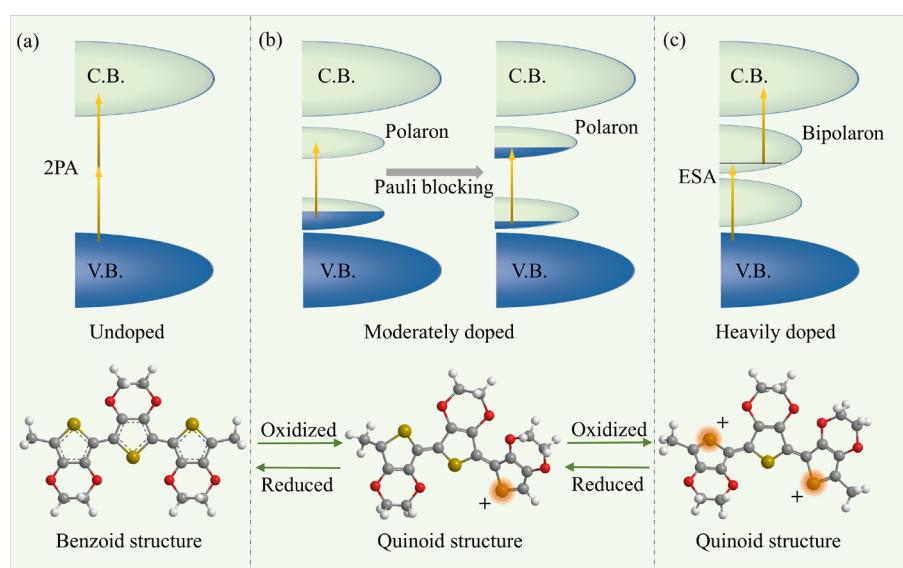

Figure 6. Proposed mechanism of the modulation of nonlinear absorption with voltage. Schematic of the density of state and molecular structure of PEDOT under different

doping states: (a) undoped, (b) moderately doped, and (c) heavily doped.

With the nature of the electron state and the origin of the NLO process revealed, the mechanism responsible for the V_A-related NLO response of the PEDOT:PSS film is proposed (Figure 6). With a V_A of -2.5 V, the PEDOT presents in the undoped state, and exhibits benzoid structure. In this case, no in-gap state can be formed, and the PEDOT shows an RSA response that can be associated with the TPA mechanism (Figure 6a). When the PEDOT is gradually oxide, it transforms into quinoid structure, and two in-gap polaron levels are formed. The lower polaron level is half-filled so that the incident laser can induce a transition from the lower polaron level to the higher polaron level. In this case, the Pauli blocking effect is prominent and the PEDOT shows a SA response (Figure 6b). With the PEDOT was further oxidized, the PEDOT exhibits abundant bipolaron states, and the bipolaron states are nearly empty. [48] In this case, the higher bipolaron level/band acts as an effective intermediate state for ESA and results in RSA (Figure 6c).

Although they are all located in the bandgap of PEDOT, polaron and bipolaron level/band result in different NLO responses, with SA for polaron-related NLO and RSA for bipolaron-related NLO. The difference arises from the detailed band structure and occupation feature of the polaron and bipolaron level. The number of polaron levels is much less than that of the bipolaron level, and the polaron level is half-filled while the bipolaron level is nearly empty.[46] Consequently, the ground state depletion and/or band filling are prominent for the transition between two polaron levels because the number of occupied polaron states is relatively small. In contrast, the amount of empty

bipolaron levels is sufficiently large so that the band-filling effect is indistinct, and these empty bipolaron levels act as intermediate states that facilitate the RSA. Briefly, the amount and filling feature of in-gap states influence heavily NLO response.

3. Conclusions

To be concluded, the third-order nonlinear absorption of the PEDOT:PSS film was electrochemically modulated. The PEDOT:PSS film exhibits RSA or SA depending on the external bias. The corresponding β_{eff} can be tuned in a range -1590 to 518 cm GW^{-1}. The doping level and energy structure of PEDOT vary with external voltage. The RSA is induced by TPA in the undoped sample, and ESA in heavily doped PEDOT, while the Pauli blocking in moderately doped PEDOT results in SA. The modulation of β_{eff} is reversible. Our results provide a facile and applicable approach for the modulation of nonparametric optical nonlinearity.

Experimental

Fabrication of PEDOT:PSS film: FTO substrates (Nippon Sheet Glass Co. Ltd.) were cleaned through successive ultrasonic treatment with detergent, acetone, ethanol, and deionized water each for 15 min. The clean FTO substrate was pretreated with UV-ozone for 10 min. The PEDOT:PSS films were deposited onto the FTO substrate by spin-coating (2300 rpm, 30 s) a PEDOT:PSS aqueous dispersion (Clevios PH1000), and the sample was then baked at 120 °C for 15 min under ambient atmosphere.

Assembly of device: The PEDOT:PSS film loaded onto the FTO substrate serves as a working electrode, and another FTO glass was mounted on the top of it using a Surlyn® membrane (DuPont). After that, the cavity was injected with ionic liquid (IL) of EMIM-BF_4 (Adamas Reagent Ltd.) and then sealed with UV-curing adhesive. The schematic structure of the PEDOT:PSS device is shown in Figure 1b.

Characterization: AFM experiment was carried out on a Bruker Dimension ICON. A SU8010 was utilized in SEM experiment. Raman spectra measurements were carried out with a inVia™ confocal Raman microscope (Renishaw, UK). The excitation source is 532 nm laser with the excitation power of 0.5 mW for *in-situ* Raman spectra.

Optical spectra and Z-scan measurement: Vis-NIR spectro-electrochemical experiments were performed using two fiber spectrometers (EK2000-Pro and EN1700, Choptics Instruments) and an electrochemistry working station (CHI760, CH Instruments). A bare device (a device assembled by two bare FTO substrates and injected with IL) was used as the back-bottom deduction to ensure that the measured data only reflect the optical absorption of PEDOT: PSS film. Single-beam nonlinear

transmittance measurements were performed on the sample through a Z-scan system. The normalized transmission of the sample was measured with a laser beam (34 fs, 800 nm) with a spot diameter of ~ 36 μm.

The effective nonlinear absorption coefficient (β_{eff}) was calculated by using the following expression:[57]

$$T_{NL}(Z) = \sum_{m=0}^{\infty} \frac{[-q_0(Z)]^m}{(m+1)^{\frac{3}{2}}},$$

$$q_0(Z) = \frac{\beta_{eff} I_0 L_{eff}}{1+(\frac{Z}{Z_0})^2}$$

$$L_{eff} = \frac{1 - e^{-\alpha_0 L}}{\alpha_0}$$

where Z is the sample coordinate, I_0 is the on-axis irradiance at focus, Z_0 is the diffraction length of the laser beam, α_0 is the linear absorption coefficient of the sample, L is the thickness.

References

(1) Eaton, D. F.; Meredith, G. R.; Miller, J. S. Molecular nonlinear optical materials—potential applications. *Adv. Mater.* **1991**, *3*, 564–565.

(2) Li, D. Q.; Ratner, M. A.; Marks, T. J. Molecular and Macromolecular Nonlinear Optical Materials. Probing Architecture/Electronic Structure/Frequency Doubling Relationships via an SCF-LCAO MECI π Electron Formalism. *J. Am. Chem. Soc.* **1988**, *110*, 1707–1715.

(3) Terhune, R. W.; Maker, P. D.; Savage, C. M. Optical Harmonic Generation in Calcite. *Phys. Rev. Lett.* **1962**, *8*, 10.

(4) Cai, W.; Vasudev, A. P.; Brongersma, M. L. Electrically Controlled Nonlinear Generation of Light with Plasmonics. *Science* **2011**, *333*, 1720–1723.

(5) Kang, L.; Cui, Y.; Lan, S.; Rodrigues, S. P.; Brongersma, M. L.; Cai, W. Electrifying photonic metamaterials for tunable nonlinear optics. *Nat. Commun.* **2014**, *5*, 4680.

(6) Lan, S.; Rodrigues, S.; Cui, Y.; Kang, L.; Cai, W. Electrically Tunable Harmonic Generation of Light from Plasmonic Structures in Electrolytes. *Nano Lett.* **2016**, *16*, 5074–5079.

(7) Ding, W.; Zhou, L.; Chou, S. Y. Enhancement and electric charge-assisted tuning of nonlinear light generation in bipolar plasmonics. *Nano Lett.* **2014**, *14*, 2822–2830.

(8) Cox, J. D.; Javier García de Abajo, F. Electrically tunable nonlinear plasmonics in graphene nanoislands. *Nat. Commun.* **2014**, *5*, 5725.

(9) Lee, K. T.; Taghinejad, M.; Yan, J.; Kim, A. S.; Raju, L.; Brown, D. K.; Cai, W. Electrically Biased Silicon Metasurfaces with Magnetic Mie Resonance for Tunable Harmonic Generation of Light. *ACS Photonics* **2019**, *6*, 2663–2670.

(10) Seyler, K. L.; Schaibley, J. R.; Gong, P.; Rivera, P.; Jones, A. M.; Wu, S.; Yan, J.; Mandrus, D. G.; Yao, W.; Xu, X. Electrical control of second-harmonic generation in a WSe_2 monolayer transistor. *Nat. Nanotechnol.* **2015**, *10*, 407–411.

(11) Wang, Y.; Xiao, J.; Zhu, H.; Li, Y.; Alsaid, Y.; Fong, K. Y.; Zhou, Y.; Wang, S.; Shi, W. Structural phase transition in monolayer $MoTe_2$ driven by electrostatic doping. *Nature* **2017**, *550*, 487–491.

(12) Klein, J.; Wierzbowski, J.; Steinhoff, A.; Florian, M.; Rösner, M.; Heimbach, F.; Müller, K.; Jahnke, F.; Wehling, T. O.; Finley, J. J. Electric-Field Switchable

Second-Harmonic Generation in Bilayer MoS$_2$ by Inversion Symmetry Breaking. *Nano Lett.* **2017**, *17*, 392–398.

(13) Soavi, G.; Wang, G.; Rostami, H.; Purdie, D. G.; Fazio, D. d.; Ma, T.; Luo, B.; Wang, J.; Ott, A. K.; Yoon, D. Broadband, electrically tunable third-harmonic generation in graphene. *Nat. Nanotechnol.* **2018**, *13*, 583–588.

(14) Ren, M. L.; Berger, J. S.; Liu, W.; Liu, G.; Agarwal, R. Strong modulation of second-harmonic generation with very large contrast in semiconducting CdS via high-field domain. *Nat. Commun.* **2018**, *9*, 186.

(15) Chen, S.; Li, K. F.; Li, G.; Cheah, K. W.; Zhang, S. Gigantic electric-field-induced second harmonic generation from an organic conjugated polymer enhanced by a band-edge effect. *Light Sci. Appl.* **2019**, *8*, 17.

(16) Li, D.; Xiong, W.; Jiang, L.; Xiao, Z.; Lu, Y. Multimodal Nonlinear Optical Imaging of MoS$_2$ and MoS$_2$-Based van der Waals Heterostructures. *ACS Nano* **2016**, *10*, 3766–3775.

(17) Li, Y.; Dong, N.; Zhang, S.; Zhang, X.; Feng, Y.; Wang, K.; Zhang, L.; Wang, J. Giant two‐photon absorption in monolayer MoS$_2$. *Laser Photonics Rev.* **2015**, *9*, 427–434.

(18) Shcherbakov, M. R.; Vabishchevich, P.; Shorokhov, A.; Chong, K. E.; Choi, D.-Y.; Staude, I.; Miroshnichenko, A. E.; Neshev, D. N.; Fedyanin, A. A.; Kivshar, Y. S. Ultrafast all-optical switching with magnetic resonances in nonlinear dielectric nanostructures. *Nano Lett.* **2015**, *15*, 6985–6990.

(19) Chen, Y.; Jiang, G.; Chen, S.; Guo, Z.; Yu, X.; Zhao, C.; Zhang, H.; Bao, Q.; Wen,

S.; Tang, D. Mechanically exfoliated black phosphorus as a new saturable absorber for both Q-switching and mode-locking laser operation. *Opt. Exp.* **2015**, *23*, 12823–12833.

(20) Cifuentes, M. P.; Powell, C. E.; Morrall, J. P.; McDonagh, A. M.; Lucas, N. T.; Humphrey, M. G.; Samoc, M.; Houbrechts, S.; Asselberghs, I.; Clays, K. Electrochemical, spectroelectrochemical, and molecular quadratic and cubic Nonlinear optical properties of alkynylruthenium dendrimers. *J. Am. Chem. Soc.* **2006**, *128*, 10819–10832.

(21) Powell, C. E.; Cifuentes, M. P.; Morrall, J. P.; Stranger, R.; Humphrey, M. G.; Samoc, M.; Luther-Davies, B.; Heath, G. A. Organometallic complexes for nonlinear optics. 30. Electrochromic linear and nonlinear optical properties of alkynylbis(diphosphine)ruthenium complexes. *J. Am. Chem. Soc.* **2003**, *125*, 602–610.

(22) Powell, C. E.; Humphrey, M. G.; Cifuentes, M. P.; Morrall, J. P.; Samoc, M.; Luther-Davies, B. Organometallic complexes for nonlinear optics. 33. Electrochemical switching of the third-order nonlinearity observed by simultaneous femtosecond degenerate four-wave mixing and pump-probe measurements. *J. Phys. Chem. A* **2003**, *107*, 11264–11266.

(23) Cifuentes, M. P.; Powell, C. E.; Humphrey, M. G.; Heath, G. A.; Samoc, M.; Luther-Davies, B. Organometallic complexes for nonlinear optics. 24. Reversible electrochemical switching of nonlinear absorption. *J. Phys. Chem. A* **2001**, *105*, 9625–9627.

(24) Feng, Q.; Li, Y.; Shi, G.; Wang, L.; Zhang, W.; Li, K.; Hou, H.; Song, Y. A photo-controllable third-order nonlinear optical (NLO) switch based on a rhodamine B salicylaldehyde hydrazone metal complex. *J. Mater. Chem. C* **2016**, *4*, 8552–8558.

(25) Malti, A.; Edberg, J.; Granberg, H.; Khan, Z. U.; Andreasen, J. W.; Liu, X.; Zhao, D.; Zhang, H.; Yao, Y.; Brill, J. W. An Organic Mixed Ion-Electron Conductor for Power Electronics. *Adv. Sci.* **2016**, *3*, 1500305.

(26) Mitraka, E.; Jafari, M. J.; Vagin, M.; Liu, X.; Fahlman, M.; Ederth, T.; Berggren, M.; Jonsson, M. P.; Crispin, X. Oxygen-induced doping on reduced PEDOT. *J. Mater. Chem. A* **2017**, *5*, 4404–4412.

(27) Asplund, M.; Thaning, E.; Lundberg, J.; Sandberg-Nordqvist, A. C.; Kostyszyn, B.; Inganäs, O.; Holst, H. V. Toxicity evaluation of PEDOT/biomolecular composites intended for neural communication electrodes. *Biomed. Mater.* **2009**, *4*, 45009.

(28) Robinson, L.; Isaksson, J.; Robinson, N. D.; Berggren, M. Electrochemical control of surface wettability of poly(3-alkylthiophenes). *Surf. Sci.* **2006**, *600*, 148–152.

(29) Backlund, F. G.; Elfwing, A.; Musumeci, C.; Ajjan, F.; Babenko, V.; Dzwolak, W.; Solin, N.; Inganas, O. Conducting microhelices from self-assembly of protein fibrils. *Soft Matter* **2017**, *13*, 4412–4417.

(30) Groenendaal, B. L.; Jonas, F.; Freitag, D.; Pielartzik, H.; Reynolds, JR. Poly(3,4-ethylenedioxythiophene) and its derivatives: Past, present, and future. *Adv. Mater.* **2000**, *12*, 481–494.

(31) Alam, M. Z.; Leon, I. de; Boyd, R. W. Large optical nonlinearity of indium tin

oxide in its epsilon-near-zero region. *Science* **2016**, *352*, 795–797.

(32) Guo, Q.; Yao, Y.; Luo, Z. C.; Qin, Z.; Xie, G.; Liu, M.; Kang, J.; Zhang, S.; Bi, G.; Liu, X. Universal Near-Infrared and Mid-Infrared Optical Modulation for Ultrafast Pulse Generation Enabled by Colloidal Plasmonic Semiconductor Nanocrystals. *ACS Nano* **2016**, *10*, 9463–9469.

(33) Guo, Q.; Cui, Y.; Yao, Y.; Ye, Y.; Yang, Y.; Liu, X.; Zhang, S.; Liu, X.; Qiu, J.; Hosono, H. A Solution-Processed Ultrafast Optical Switch Based on a Nanostructured Epsilon-Near-Zero Medium. *Adv. Mater.* **2017**, *29*, 1700754.

(34) Tian, X.; Luo, H.; Wei, R.; Zhu, C.; Guo, Q.; Yang, D.; Wang, F.; Li, J.; Qiu, J. An Ultrabroadband Mid-Infrared Pulsed Optical Switch Employing Solution-Processed Bismuth Oxyselenide. *Adv. Mater.* **2018**, *30*, 1801021.

(35) Zhang, X.; Liu, S.; Tan, D.; Xian, Y.; Zhang, D.; Zhang, Z.; Liu, Y.; Liu, X.; Qiu, J. Photochemically Derived Plasmonic Semiconductor Nanocrystals as an Optical Switch for Ultrafast Photonics. *Chem. Mater.* **2020**, *32*, 3180–3187.

(36) Zhang, S.; Dong, N.; McEvoy, N.; O'Brien, M.; Winters, S.; Berner, N. C.; Yim, C.; Li, Y.; Zhang, X.; Chen, Z. Direct Observation of Degenerate Two-Photon Absorption and Its Saturation in WS_2 and MoS_2 Monolayer and Few-Layer Films. *ACS Nano* **2015**, *9*, 7142–7150.

(37) Wang, K.; Szydłowska, B. M.; Wang, G.; Zhang, X.; Wang, J. J.; Magan, J. J.; Zhang, L.; Coleman, J. N.; Wang, J.; Blau, W. J. Ultrafast Nonlinear Excitation Dynamics of Black Phosphorus Nanosheets from Visible to Mid-Infrared. *ACS Nano* **2016**, *10*, 6923–6932.

(38) Wang, K.; Wang, J.; Fan, J.; Lotya, M.; O'Neill, A.; Fox, D.; Feng, Y.; Zhang, X.; Jiang, B.; Zhao, Q. Ultrafast Saturable Absorption of Two-Dimensional MoS$_2$ Nanosheets. *ACS Nano* **2013**, *7*, 9260–9267.

(39) Kumar, S.; Anija, M.; Kamaraju, N.; Vasu, K. S.; Subrahmanyam, K. S.; Sood, A. K.; Rao, C. N. R. Femtosecond carrier dynamics and saturable absorption in graphene suspensions. *Appl. Phys. Lett.* **2009**, *95*, 191911.

(40) Elim, H. I.; Ji, W.; Ng, M. T.; Vittal, J. J. AgInSe$_2$ nanorods: A semiconducting material for saturable absorber. *Appl. Phys. Lett.* **2007**, *90*, 33106.

(41) Elim, H. I.; Yang, J.; Lee, J. Y.; Mi, J.; Ji, W. Observation of saturable and reverse-saturable absorption at longitudinal surface plasmon resonance in gold nanorods. *Appl. Phys. Lett.* **2006**, *88*, 83107.

(42) Gallagher, K. G.; Croy, J. R.; Balasubramanian, M.; Bettge, M.; Abraham, D. P.; Burrell, A. K.; Thackeray, M. M. Correlating hysteresis and voltage fade in lithium- and manganese-rich layered transition-metal oxide electrodes. *Electrochem. Commun.* **2013**, *33*, 96–98.

(43) Garreau, S.; Duvail, J. L.; Louarn, G. Spectroelectrochemical studies of poly(3,4-ethylenedioxythiophene) in aqueous medium. *Synth. Met.* **2001**, *125*, 325–329.

(44) Yang, C. S.; Shang, D. S.; Liu, N.; Shi, G.; Shen, X.; Yu, R. C.; Li, Y. Q.; Sun, Y. A Synaptic Transistor based on Quasi-2D Molybdenum Oxide. *Adv. Mater.* **2017**, *29*, 1700906.

(45) Louarn, G.; Trznadel, M.; Buisson, J. P.; Laska, J.; Pron, A.; Lapkowski, M.; Lefrant, S. Raman Spectroscopic Studies of Regioregular Poly(3-alkylthiophenes).

J. Phys. Chem. **1996**, *100*, 12532–12539.

(46) Heeger, A. J. Charge Storage in Conducting Polymers: Solitons, Polarons, and Bipolarons. *Polym. J.* **1985**, *17*, 201–208.

(47) Gueye, M. N.; Carella, A.; Faure-Vincent, J.; Demadrille, R.; Simonato, J. P. Progress in understanding structure and transport properties of PEDOT-based materials: A critical review. *Prog. Mater. Sci.* **2020**, *108*, 100616.

(48) Patil, A. O.; Heeger, A. J.; Wudl, F. Optical-Propertoes of Conducting Polymers. *Chem. Rev.* **1988**, *88*, 183–200.

(49) Bubnova, O.; Khan, Z. U.; Malti, A.; Braun, S.; Fahlman, M.; Berggren, M.; Crispin, X. Optimization of the thermoelectric figure of merit in the conducting polymer poly(3,4-ethylenedioxythiophene). *Nat. Mater.* **2011**, *10*, 429–433.

(50) Gustafsson, J. C.; Liedberg, B.; Inganfis, O. In situ spectroscopic investigations of electrochromism and ion transport in a poly (3,4-ethylenedioxythiophene) electrode in a solid state electrochemical cell. *Solid State Ionics* **1994**, *69*, 145–152.

(51) Chung, T. C.; Kaufman, J. H.; Heeger, A. J.; Wudl, F. Charge storage in doped poly(thiophene): Optical and electrochemical studies. *Phys. Rev. B* **1984**, *30*, 702.

(52) Zitter, R. N. Saturated Optocal Absorption Through Band Filling in Semiconductors. *Appl. Phys. Lett.* **1969**, *14*, 73–74.

(53) Sachs, M.; Park, J. S.; Pastor, E.; Kafizas, A.; Wilson, A. A.; Francas, L.; Gul, S.; Ling, M.; Blackman, C.; Yano, J. Effect of oxygen deficiency on the excited state kinetics of WO_3 and implications for photocatalysis. *Chem. Sci.* **2019**, *10*, 5667–5677.

(54) Barroso, M.; Pendlebury, S. R.; Cowan, A. J.; Durrant, J. R. Charge carrier trapping, recombination and transfer in hematite (alpha-Fe_2O_3) water splitting photoanodes. *Chem. Sci.* **2013**, *4*, 2724–2734.

(55) Correa, D. S.; Boni, L. de; Misoguti, L.; Cohanoschi, I.; Hernandez, F. E.; Mendonca, C. R. Z-scan theoretical analysis for three-, four- and five-photon absorption. *Opt. Commun.* **2007**, *277*, 440–445.

(56) Zhang, Q.; Liu, X.; Utama, M. I. B.; Xing, G.; Sum, T. C.; Xiong, Q. Phonon-Assisted Anti-Stokes Lasing in ZnTe Nanoribbons. *Adv. Mater.* **2016**, *28*, 276–283.

(57) Sheik-Bahae, M.; Said, A. A.; Wei, T. H.; Hagan, D. J.; Van Stryland, E. W. Sensitive measurement of optical nonlinearities using a single beam. *IEEE J. Quantum Electron.* **1990**, *26*, 760–769.